Sensors and Materials, Vol. 36, No. 10 (2024) 4179–4191
MYU Tokyo

S & M 3793

Using the Finite Element Simulation Software Ansys to Analyze the Stress and Strain Generated in the Eyeball due to Pressure When Subjected to Compression

Sufang Cai,[1] Pei-Chang Wu,[2,3] Chih-Chung Cheng,[4]
Chao-Ming Hsu,[4] Linda Yi-Chieh Poon,[2,3*] and Cheng-Fu Yang[5,6**]

[1]Rehabilitation Hospital Affiliated with Fujian University of Traditional Chinese Medicine, Fuzhou 350001, China
[2]Department of Ophthalmology, Kaohsiung Chang Gung Memorial Hospital, Kaohsiung 833, Taiwan
[3]School of Medicine, Chang Gung University, Taoyuan 333, Taiwan
[4]Department of Mechanical Engineering, National Kaohsiung University of Science and Technology, Kaohsiung 807, Taiwan
[5]Department of Chemical and Materials Engineering, National University of Kaohsiung, Kaohsiung 811, Taiwan
[6]Department of Aeronautical Engineering, Chaoyang University of Technology, Taichung 413, Taiwan

(Received April 30, 2024; accepted September 5, 2024)

Keywords: stress and strain, intraocular pressure (IOP), fluid–structure interaction, applanation tonometry, ocular biomechanics

In this study, we conducted stress and strain analyses on the eyeball under pressure using the finite element simulation software Ansys. The eyeball model was constructed using SolidWorks, and additionally, it simulates a contact-type tonometer, applying pressure to the eyeball through probe force variations and calculating the pressure changes inside the eyeball. Initially, the cornea, sclera, ciliary body, suspensory ligaments, aqueous humor, and vitreous humor were combined using SolidWorks. Subsequently, the model was imported into Ansys for meshing, boundary setting, and simulation calculation. Finally, the analysis results were extracted using the Ansys postprocessor and the simulated data were validated against actual measurement data to ensure accuracy. Material properties necessary for the eyeball under pressure analyses were configured, with the Mooney–Rivlin hyperelastic material being selected. During compression, the cornea and sclera primarily absorbed the concentrated load after compression. Pressure was applied using a probe to observe variations in stress and strain concerning the applied force and intraocular pressure. Three probe materials (rubber, titanium alloy, and glass) were chosen for comparative simulation analyses.

1. Introduction

The ciliary body is situated between the iris and the choroid, connected to the crystalline lens via suspensory ligaments. It plays a crucial role in adjusting the shape and thickness of the lens

*Corresponding author: e-mail: lindap@cgmh.org.tw
**Corresponding author: e-mail: cfyang@nuk.edu.tw
https://doi.org/10.18494/SAM5102

ISSN 0914-4935
https://myukk.org/

to achieve an appropriate focal length. Additionally, the ciliary body secretes a fluid called aqueous humor, which nourishes the cornea and maintains intraocular pressure (IOP). Surrounding the lens is an elastic tissue called suspensory ligaments, also known as zonular fibers, which attach to the ciliary body, keeping the lens in place. As the ciliary muscle contracts and relaxes, it adjusts the curvature of the lens, facilitating the normal refractive function of the eye. Under normal physiological conditions, when focusing on near objects, the ciliary muscle contracts while the suspensory ligaments relax, causing the lens to move forward and increase in curvature, thus enhancing the eye's refractive power. However, defects in the suspensory ligaments can lead to an imbalance in suspensory forces, resulting in the abnormal positioning of the lens and a rapid increase in IOP. In the past, Czudowska *et al.* found from numerous large-scale epidemiological studies that elevated IOP or fluctuations in IOP, as well as high myopia, are both exacerbating factors for glaucoma.[1,2] However, the relationship between IOP and myopia in relation to glaucoma remains unclear.[3-4]

One of the reasons for the difficulty in defining the relationship between IOP and myopia is that in diagnosing myopic patients with glaucoma, most patients have IOP within the normal range (less than 21 mmHg), with fewer patients having elevated IOP.[2] In medical diagnosis and eye-related surgeries, IOP values serve as crucial auxiliary indicators. The eye, being one of the most delicate structures in the human body, necessitates precise and safe measurement, making it an important consideration. Theoretically, measuring IOP involves using a manometer to directly measure the actual pressure within the eye. This is performed by inserting a tube filled with liquid into a corneal incision, and by utilizing the principle of fluid communication, the height of the liquid column in the tube directly indicates IOP. Although this method yields accurate results, it is clearly not practical for routine clinical use. Presently, clinical tonometers apply external force to the eye and measure its response indirectly. The measurement of IOP is an essential method for assessing eye health, particularly in detecting conditions such as glaucoma. Common methods for measuring IOP include the following:

(a) Noncontact tonometry: Also known as air-puff tonometry, this method involves directing a gentle puff of air onto the eye while the patient rests their head on a support. The instrument measures the rebound of the air puff to calculate IOP.[5]
(b) Applanation tonometry: This is another common method where a special instrument, called a tonometer, gently touches the surface of the eye to measure IOP. The most common type of applanation tonometry is Goldmann applanation tonometry.

Before conducting IOP measurements, it is common to use eye drops, especially for noncontact measurements, to protect the eyes from the airflow or instrument contact.[6] Additionally, patients are typically instructed to focus and keep their eyes still during measurement to obtain accurate results. Finally, IOP measurement should be part of routine eye health assessments and preferably conducted under the supervision of an ophthalmologist. Applanation tonometry offers several advantages over noncontact methods. First, it tends to provide results more accurate than those obtained by noncontact tonometry. Additionally, it is versatile and suitable for various eye conditions, including postsurgical situations. However, there are drawbacks to applanation tonometry. It requires direct contact with the eye, which may induce slight discomfort in patients and necessitates more technical expertise to ensure precise

measurements. Furthermore, the measurement process typically takes longer than noncontact methods. Noncontact tonometry, on the other hand, eliminates the need for direct contact with the eye, reducing discomfort and minimizing irritation to the cornea. It also offers rapid measurements, often completed within seconds, and is generally easier to operate for both patients and practitioners.

Nevertheless, noncontact tonometry has its limitations. It may lack some accuracy compared with applanation tonometry, particularly in specific eye conditions or postsurgical scenarios. Additionally, external environmental factors such as airflow can interfere with measurements, necessitating controlled environments for accurate results. To reduce contact measurement time and increase accuracy, in this study, we utilized the finite element simulation software Ansys to analyze the stress and strain produced in the eyeball when subjected to pressure.[7–9] The eyeball analysis model was constructed using SolidWorks. Initially, various components such as the sclera, cornea, ciliary body, suspensory ligaments, aqueous humor, and vitreous humor were combined using SolidWorks drafting software. Subsequently, the model was imported into Ansys for meshing, boundary setting, and simulation calculations. Finally, the analysis results were extracted using the Ansys postprocessor. Throughout this process, the simulated data were compared with actual measurements to verify the accuracy of the analysis. This approach offers several advantages. First, it enables researchers to explore the intricate mechanical behavior of the eyeball under different pressure conditions without the constraints of physical experiments, thereby saving time and resources. Additionally, by integrating various anatomical structures and physiological parameters into the simulation model, a more comprehensive understanding of IOP dynamics can be achieved. Moreover, the validation process against real-world measurements ensures the reliability and fidelity of the simulation results, enhancing their applicability in clinical settings and surgical planning.

2. Methodology

The size of the eyeball varies from person to person. In this study, eyeball dimensions were selected from references, representing typical dimensions of adult eyeballs. First, using SolidWorks drawing software, the sclera, cornea, ciliary body, suspensory ligaments, aqueous humor, and vitreous humor were combined and drawn.[10,11] Ansys offers a wide range of analysis modes, each tailored to address specific types of problem. The Mesh module of Ansys was utilized for grid generation, as illustrated in Figs. 1(a) and 1(b). In the simulation process, the Lagrangian method involves grid deformation along with material deformation, making it the most efficient and accurate approach for structural modeling. However, in simulations where materials undergo extreme deformation, such as fluid or gas flow around obstacles, the elements may undergo significant deformation. Eventually, elements may become distorted, encompassing structures such as the cornea, sclera, ciliary body, suspensory ligaments, and lens. On the other hand, the Eulerian grid remains stationary throughout the simulation and can accommodate large material deformations. For materials that are prone to significant deformations, such as aqueous humor and vitreous humor, the Eulerian method is preferable. Figure 2 depicts the differences between simulations conducted using the Lagrangian and Eulerian methods.

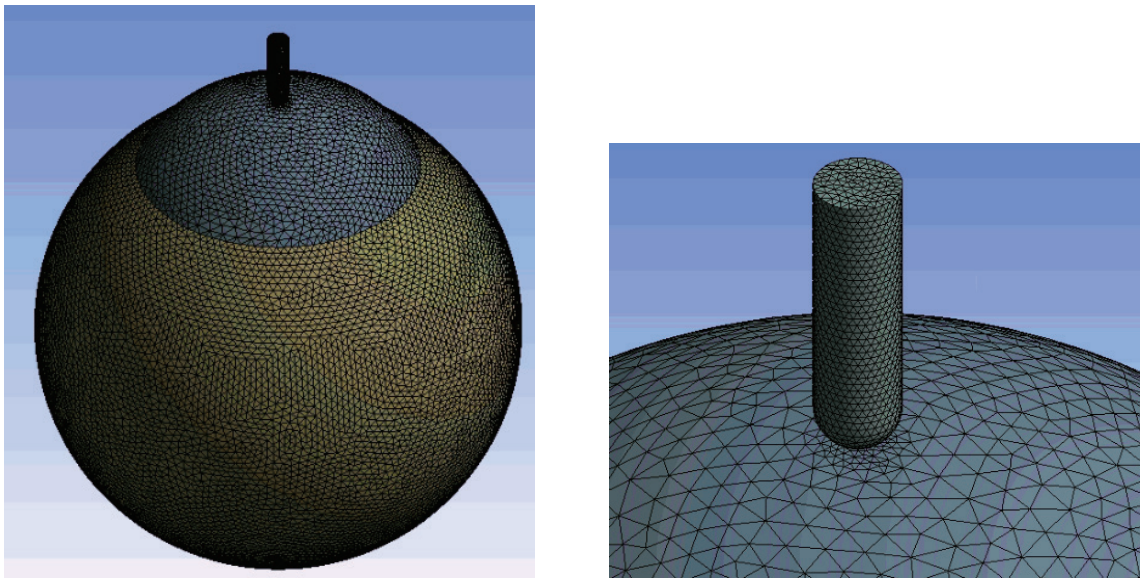

(a) (b)

Fig. 1. (Color online) Diagram for eye mesh.

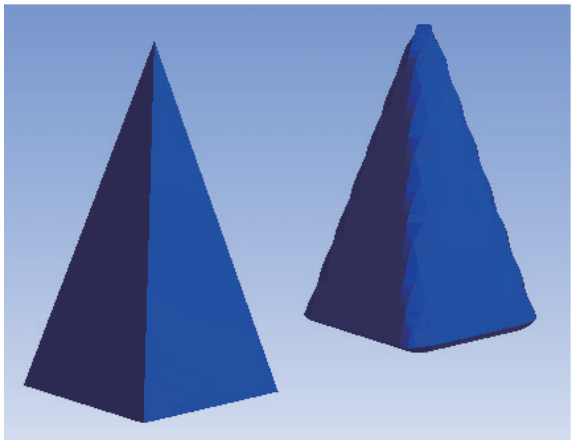

Fig. 2. (Color online) Differences between simulations conducted using the Lagrangian (left) and Eulerian methods (right).

The number of nodes represents the total number of nodes in the elements. Software calculates stress, strain, or various field quantities at the nodes of the elements, while the values at other points of the elements are obtained through the interpolation of nodal field quantities. Ansys provides both first-order (linear) and second-order (quadratic) elements, each differing in the number of nodes. Before meshing, geometric models are processed using Ansys's Design Modeler to ensure the computational integrity of each surface. This is primarily carried out to avoid poor mesh quality or interference issues that could lead to significant errors or even computational failure. In Ansys meshing, for structured meshes, the number of mesh nodes per adjacent total mesh is defined within a range. The eye in this study is a complex structure,

making mesh generation challenging. Therefore, when meshing the intricate model of the eye, we employ tetrahedral and triangular elements. The advantage of using these elements lies in their versatility, as they can be easily generated on any model.

First, it is necessary to create an analysis step in the Analysis Step module. Ansys provides users with a selection of analysis steps for various types of problem. After creating the analysis step, detailed settings must be applied. In this study, we first set the relationship between the cornea and sclera tissues as a single entity. The contact surface between the probe and the cornea was set to have no friction. The probe was fixed, with the displacement along the *X*- and *Z*-axes set to 0, whereas the displacement along the *Y*-axis was set to Free. Rotations along the *X*-, *Y*-, and *Z*-axes were set to 0. The probe was aligned with the cornea of the eyeball, and the direction of force applied by the probe is as shown in Fig. 3. To further optimize this process, additional considerations could be made regarding the material properties, boundary conditions, and simulation parameters to ensure an accurate representation of the physical system under investigation. Additionally, discussing the rationale behind each setting and its implications for the analysis results can provide insights into the modeling decisions made and their relevance to the research objectives.

Meshing is a critical stage in numerical simulations, as it directly impacts the accuracy of analysis results and computation time. Generally, the higher the number of elements in a finite element model, the higher the accuracy, but excessive element counts can lead to increased computation time. To achieve a balance between solution accuracy and computation time, it is essential to perform convergence analysis on the model. In this study, we conducted the convergence analysis by establishing different element counts and utilizing the remeshing function for mesh refinement. The overall model focused on the contact point between the

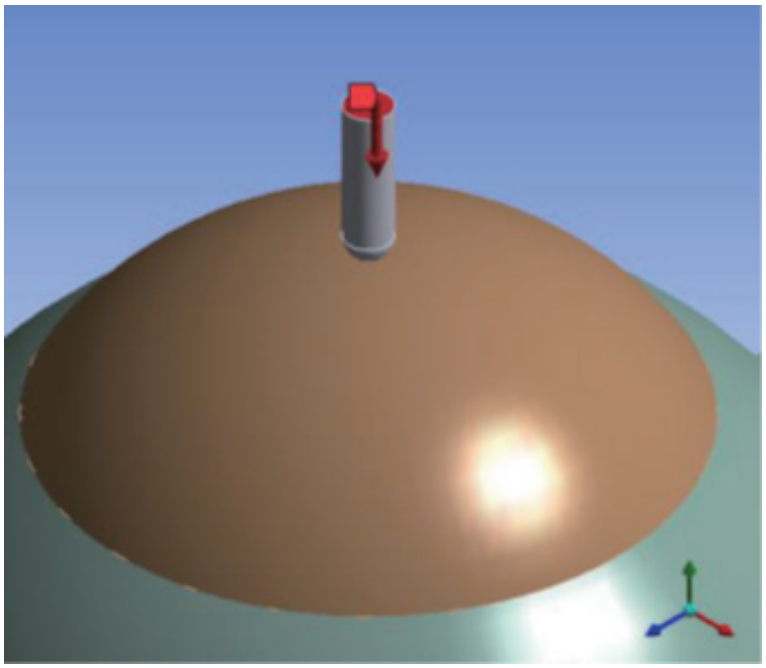

Fig. 3. (Color online) Diagram illustrating the contact surface between the cornea and the probe.

cornea and the probe in a supine position for convergence analysis, as depicted in Fig. 1, which represents the data extraction points. Since the model in this study involves curved surfaces, a baseline of 200 thousand elements was set to achieve the minimum element count for solver compatibility. The element count was gradually increased, and from the analysis data, it was observed that the stress experienced by the cornea remained within the 1% numerical error range when the element count ranged from 400 thousand to 500 thousand. Therefore, an element count of 400 thousand was chosen for the analysis. To further enhance this process, considerations could be made regarding mesh quality, element type, and distribution to ensure the optimal convergence behavior and accuracy of results. Additionally, validating the chosen element count against experimental data or benchmark cases can provide confidence in the simulation outcomes. Furthermore, discussing the implications of mesh refinement strategies on computational efficiency and solution accuracy can contribute to a deeper understanding of the simulation methodology employed.

3. Simulation Results and Discussion

The loads and boundary conditions are set through the load module. These loads and boundary conditions are associated with the analysis step. Since IOP refers to the pressure exerted on the inner wall of the eyeball, the loads are set to simulate the pressure exerted on the sclera, as illustrated in Fig. 4. In the loads section, the probe is subjected to forces of 9.81, 19.62,

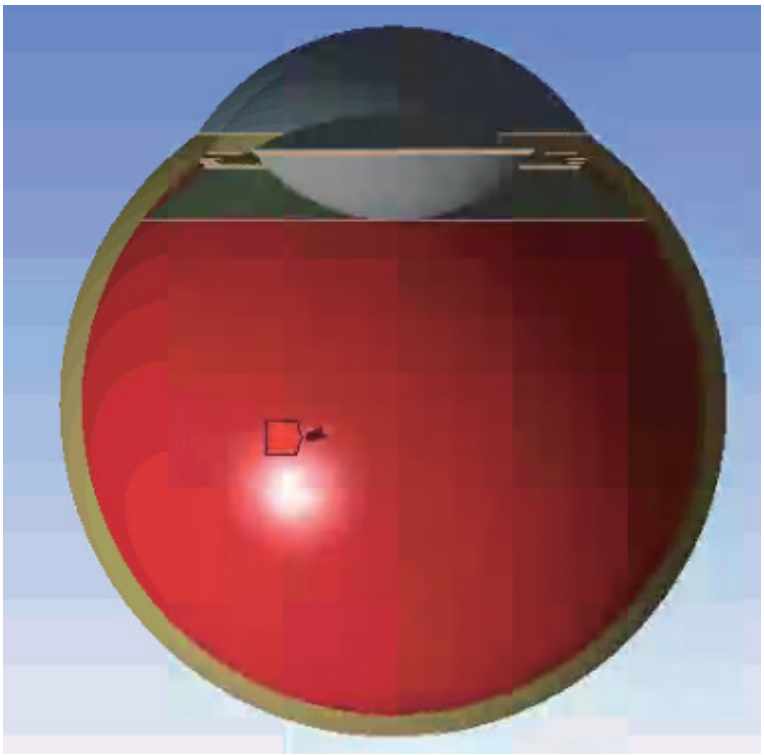

Fig. 4. (Color online) Diagram illustrating the application of pressure on the inner walls of the eyeball.

29.43, 39.24, and 49.05 mN, corresponding to IOPs of 10, 20, 30, 40, and 50 mmHg, respectively, as shown in Table 1. The IOP settings are 1.33, 2.66, 3.99, 5.32, and 6.65 kPa. Additionally, three different postures of the eyeball are simulated. To enhance this process, it is essential to consider the distribution and application of loads and boundary conditions to accurately represent the physiological conditions and biomechanical responses of the eye. Moreover, validating these simulation settings against experimental data or clinical observations can improve the reliability and relevance of the simulated outcomes. Furthermore, discussing the significance of IOP variations and their implications for ocular biomechanics can enrich the understanding of the simulated scenarios and their potential clinical implications.

The data extraction points for corneal pressure are depicted in Fig. 5(a), positioned at the site of pressure application to capture numerical variations throughout the pressure application process. The region for optic nerve data extraction is delineated by the green area in Fig. 5(b). Tasman and Jaeger found that the optic nerve's position is approximately 3−4 mm from the central point, with an elliptical area of 1.5 × 2 mm diameter.[12] This region was used to simulate the optic nerve's position on the eyeball. On the basis of this significant finding, we simulated this specific area to represent the position of the optic nerve on the eyeball.

Table 1
Keratoplate tonometer measurement chart.

Pressure (mmHg)	Force (mN)	Pressure (kPa)
10	9.81	1.33
20	19.62	2.66
30	29.43	3.99
40	39.24	5.32
50	49.05	6.65

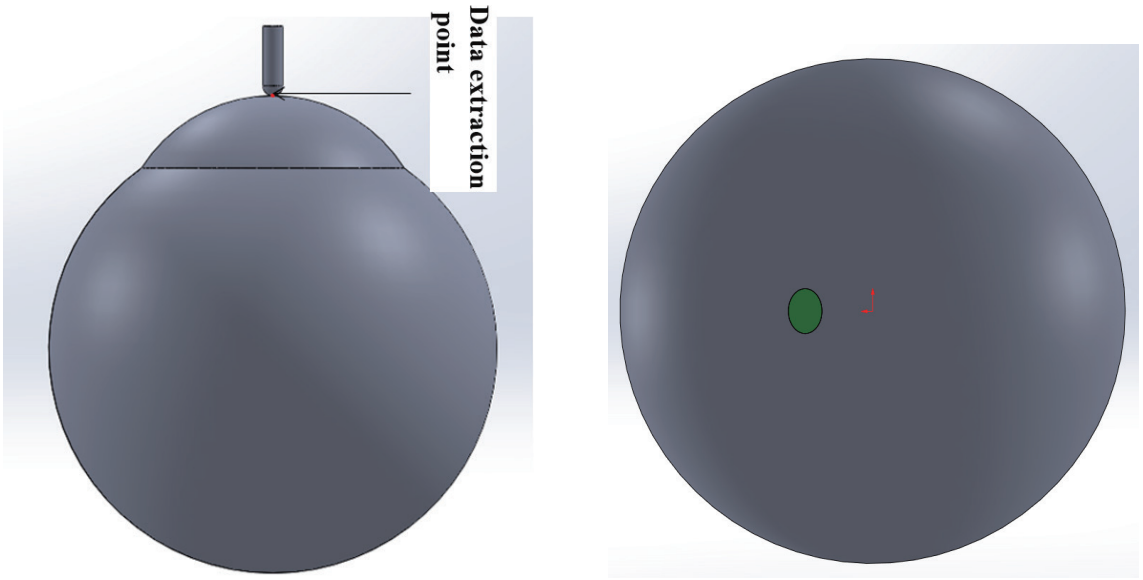

(a) (b)

Fig. 5. (Color online) (a) Data extraction points for corneal pressure and (b) region of optic nerve data extraction.

It would be beneficial to discuss the implications of the observed stress and strain distributions on corneal biomechanics and potential implications for ocular health. Additionally, comparing these findings with experimental data or clinical observations can validate the accuracy of the simulation results and provide insights into the applicability of the simulated scenarios to real-world conditions. Figures 6(a) and 6(b) illustrate the distribution of equivalent stress on the cornea under pressure. From these figures, it is discernible that the stress distribution is concentrated at the contact region between the probe and the cornea. Figures 7(a) and 7(b) represent the strain distribution on the cornea under pressure. Similar to the stress distribution, the strain distribution is observed to be concentrated at the same region as the stress distribution.

The strain distribution corresponds to the stress distribution. Figure 8 illustrates the variation in corneal equivalent stress and strain due to different forces applied to the probe, with the probe material being rubber and the posture being standing. From Fig. 8, it is evident that following corneal pressure, the variation in equivalent stress ranges from 0.11 to 0.237 MPa, while the strain varies from 0.13 to 0.195 mm/mm. The relationship between the applied force magnitude and the changes in equivalent stress and strain appears to be linear. Figure 9 shows the variations in equivalent stress and strain at the optic nerve location. The equivalent stress ranges from 1.7 to 2.9 kPa, while the strain varies between 5.5×10^{-4} and 5.8×10^{-4} mm/mm, stabilizing over time. This indicates that the optic nerve experiences minimal impact during corneal pressure and changes in IOP. These analyses shed light on the biomechanical responses of the cornea and optic nerve to pressure variations, providing insights into their resilience and stability under external loads. Further investigation into the underlying mechanisms governing these responses can enhance our understanding of ocular biomechanics and contribute to the development of more effective diagnostic and treatment strategies for ocular disorders.

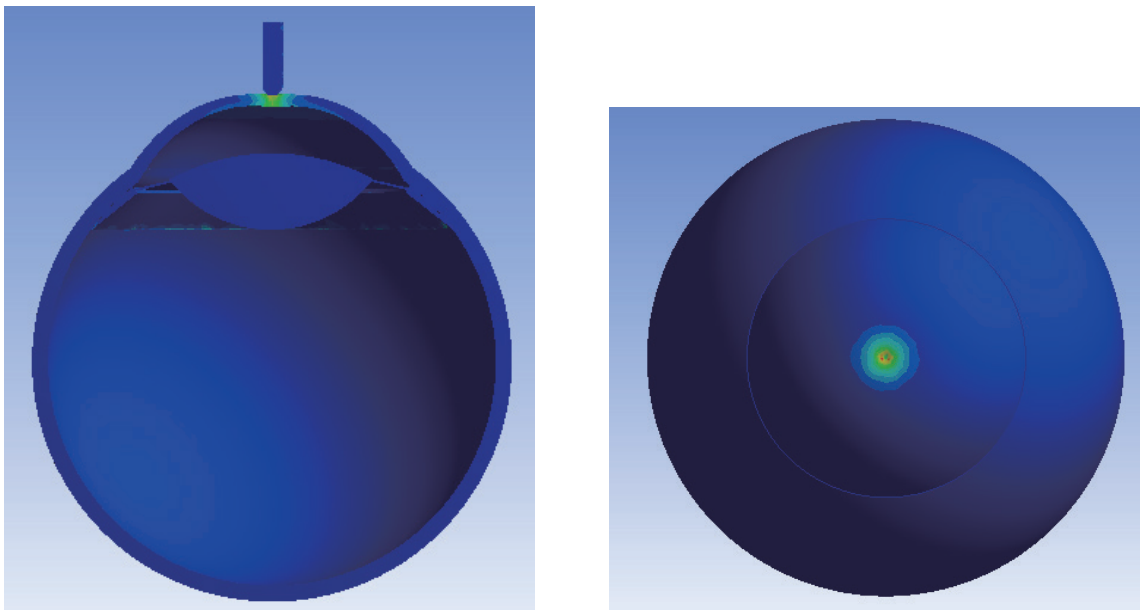

(a) (b)

Fig. 6. (Color online) Corneal pressure Von-Mises distribution chart: (a) frontal and (b) top views.

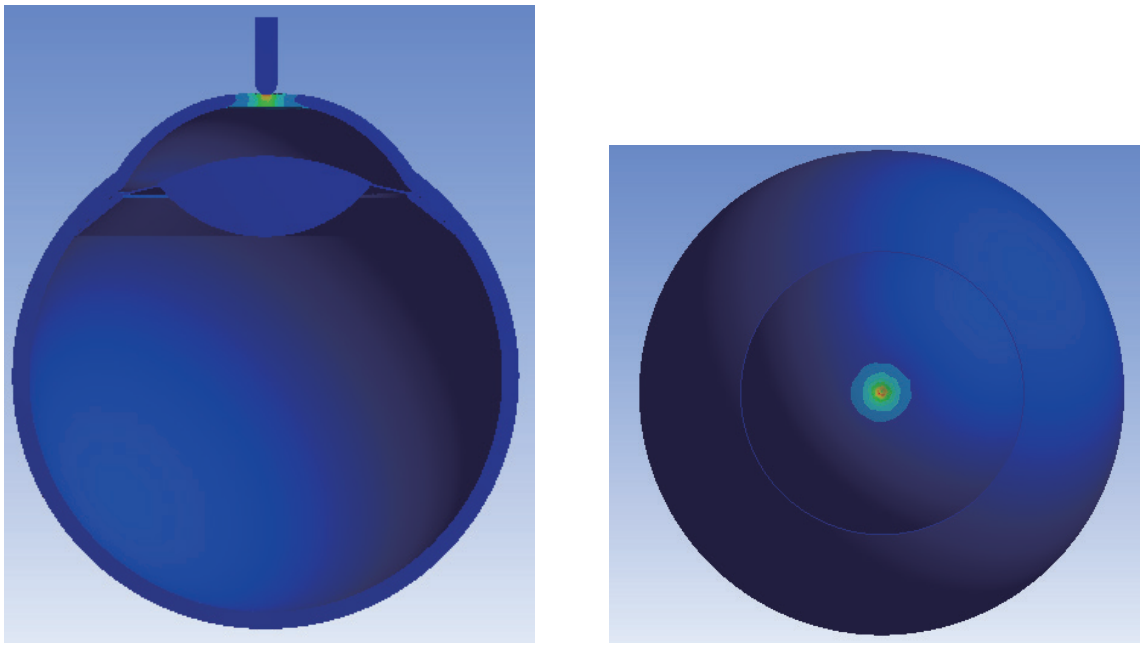

(a) (b)

Fig. 7. (Color online) Corneal pressure strain distribution chart: (a) frontal and (b) top views.

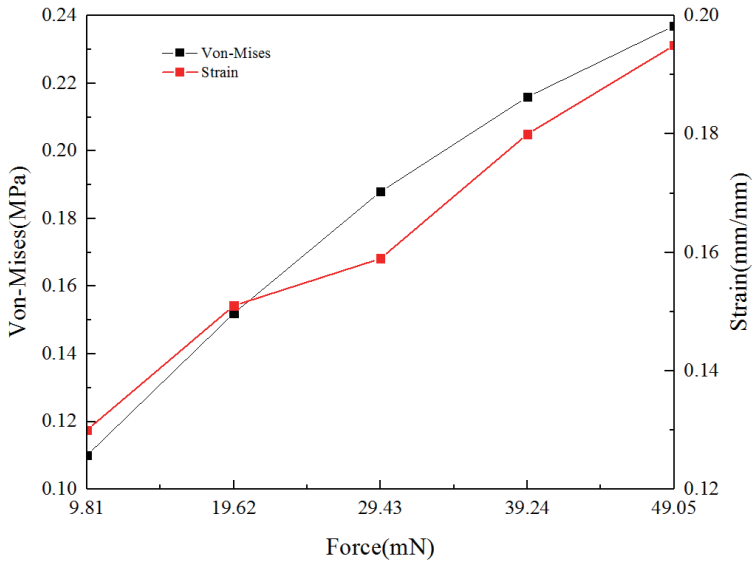

Fig. 8. (Color online) Variations in corneal equivalent stress and strain under different forces applied by the rubber probe.

Figure 10 illustrates the variations in equivalent stress and strain on the cornea when subjected to pressure with a probe made of titanium alloy. The progression of equivalent stress ranges from 0.087 to 0.195 MPa, while strain varies from 0.091 to 0.15 mm/mm. In Fig. 11, the equivalent stress and strain variations at the optic nerve position are shown, with equivalent

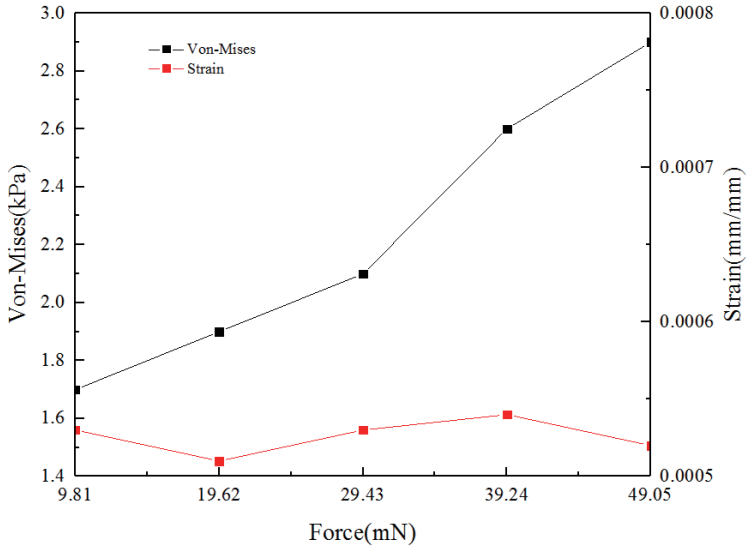

Fig. 9. (Color online) Variations in equivalent stress and strain at the optic nerve location under different forces applied by the rubber probe.

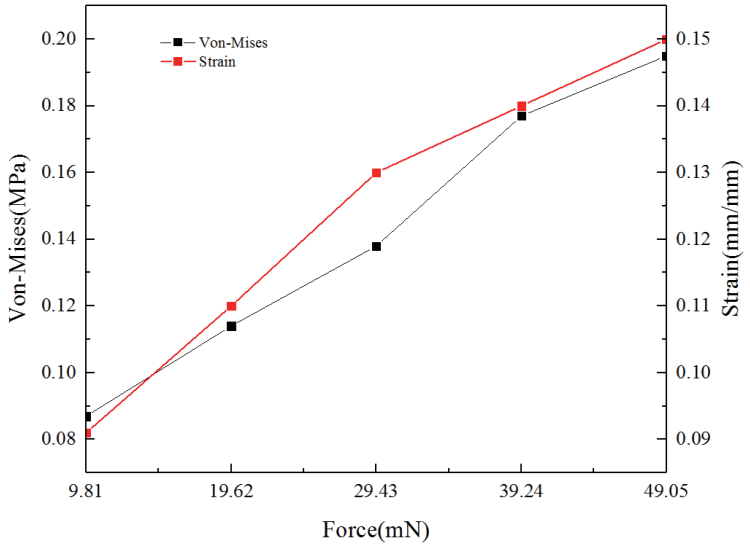

Fig. 10. (Color online) Variations in corneal equivalent stress and strain under different forces applied by the titanium alloy probe.

stress ranging from 1.5 to 2.8 kPa and strain ranging from 5.4×10^{-4} to 5.8×10^{-4} mm/mm. Conversely, Fig. 12 shows the equivalent stress and strain variations on the cornea when pressed with a probe made of glass. The range of equivalent stress shifts from 0.105 to 0.203 MPa, while strain varies from 0.1 to 0.183 mm/mm. Figure 13 then illustrates the equivalent stress and strain variations at the optic nerve position, with equivalent stress ranging from 1.6 to 2.9 kPa and strain ranging from 5.5×10^{-4} to 5.8×10^{-4} mm/mm.

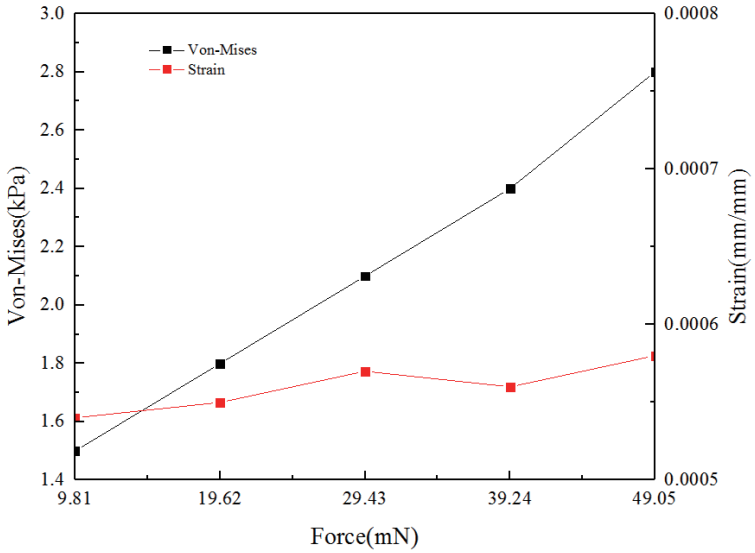

Fig. 11. (Color online) Variations in equivalent stress and strain at the optic nerve position under different forces applied by the titanium alloy probe.

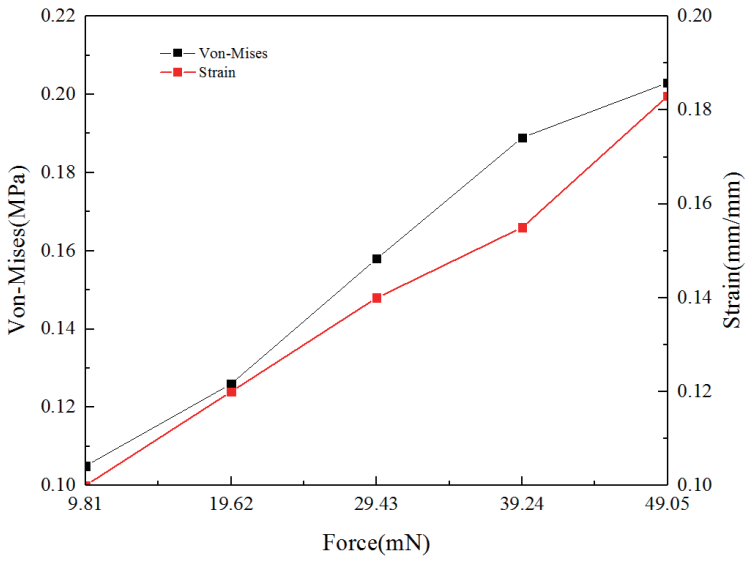

Fig. 12. (Color online) Variations in corneal equivalent stress and strain under different forces applied by the glass probe.

Comparison of Figs. 8, 10, and 12 reveals slight discrepancies in the equivalent stress and strain experienced by the cornea due to variations in probe material. These differences arise from the effects of gravitational conditions on stress and strain during simulation. When the same force is applied to materials of different weights, lighter materials exhibit greater displacement, leading to variations in equivalent stress. Thus, the choice of probe material can significantly affect the mechanical response of the cornea under pressure. When simulating the variations in stress and strain in response to different levels of force applied to the eyeball and

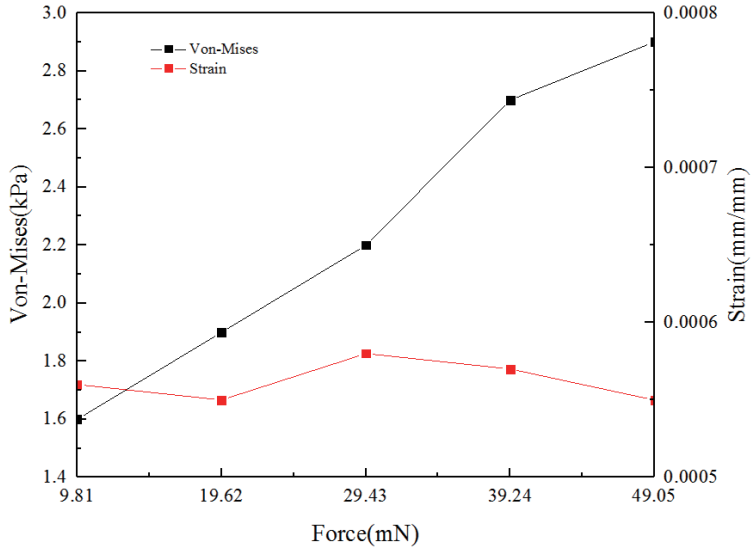

Fig. 13. (Color online) Variations in equivalent stress and strain at the optic nerve position under different forces applied by the glass probe.

eye pressure using rubber, titanium alloy, and glass, there may be several reasons for the differences in the results, as listed below.

(1) Different material properties: Rubber, titanium alloy, and glass are different materials with varying elastic moduli, tensile strengths, and other physical properties. These differences will result in varying levels of strain and stress distributions under the same applied force.

(2) Disparity in elastic modulus: The elastic modulus, which represents a material's ability to deform elastically under stress, differs significantly among materials. Rubber typically has a lower elastic modulus, while titanium alloy and glass have higher values. This means that rubber will undergo greater deformation under the same force, whereas titanium alloy and glass will experience less deformation.

(3) Material toughness and brittleness: Rubber is typically a resilient elastic material capable of withstanding a certain degree of deformation without fracturing. Titanium alloy and glass may be more brittle, prone to fracture or develop cracks when subjected to external forces, which could affect material behavior.

These factors combined contribute to the observed differences in the behavior of rubber, titanium alloy, and glass when simulating variations in stress and strain in response to different levels of force applied to the eyeball and eye pressure.

4. Conclusions

In this study, we utilized an eyeball model and finite element analysis to simulate IOP by incorporating the material properties of the eyeball. Our aim was to examine the stress conditions of the cornea during IOP measurement with three different materials and to investigate variations in IOP under different loading conditions. Additionally, we discussed the

values of stress (Von-Mises) and strain after compression and rotation. No matter what material the probe is made of, the corneal equivalent stress and strain both exhibit linear variations. Among the three probe materials, rubber induces the highest strain and the strain induced at the optic nerve position ranges from 0.0005 to 0.0006. The analysis of the eyeball under pressure revealed that stress and strain were concentrated at the contact point between the probe and the cornea. It was found that this pressure did not cause damage to the optic nerve behind the eyeball. Furthermore, different materials of the probe did not affect the measured IOP.

Acknowledgments

This work was supported by the Xiamen Science and Technology Plan Project - Industry University Research Project (No. 2023CXY0416), the Natural Science Foundation Project of Fujian Provincial Department of Science and Technology (No. 2023J01976), and Fujian Provincial Young and Middle-aged Teacher Education Project (No. JAT200455).

References

1 M. A. Czudowska, W. D. Ramdas, R. C. W. Wolfs, A. Hofman, P. T. V. M. De Jong, J. R Vingerling, and N. M. Jansonius: Ophthalmology **117** (2010) 1705.
2 M. W. Marcus, M. M. de Vries, F. G. Junoy Montolio, and N. M. Jansonius: Ophthalmology **118** (2011) 1989.
3 R. T Chang and K. Singh: Curr. Opin. Ophthalmol. **24** (2013) 96.
4 Y. C. Tham, T. Aung, Q. Fan, S. M. Saw, R. G. Siantar, T. Y. Wong, and C. Y. Cheng: Sci. Rep. **6** (2016) 19320.
5 B. Audrey Nguyen, M. A. Reilly, and C. J. Roberts: Exp. Eye Res. **191** (2020) 107904.
6 C. Whitford, A. Joda, S. Jones, F. Bao, P. Rama, and A. Elsheikh: Eye Vision **3** (2016) 21.
7 T. Rossi, B. Boccassini, L. Esposito, M. Iossa, A. Ruggiero, C. Tamburrelli, and N. Bonora: Investig. Ophthalmol. Vis. Sci. **52** (2011) 3994.
8 A. Karimi, R. Razaghi, M. Navidbakhsh, T. Sera, and S. Kudo: Injury Int. J. Care Injured **47** (2016) 1042.
9 D. M. Munoz Sarmiento, O. L. Rodríguez Montano, J. D. Alarcon Castiblanco, and C. J. Cortes Rodríguez: Heliyon **9** (2023) e13634.
10 J. C. Barry, M. Dunne, and T. Kirschkamp: Ophthal. Physiol. Opt. **21** (2001) 450.
11 I. A. Sigal, J. L. Grimm, J. S. Schuman, L. Kagemann, H. Ishikawa, and G. Wollstein: IEEE Trans. Med. Imaging **33** (2014) 1381.
12 W. Tasman and E. A. Jaeger: Duane's Ophthalmology (Lippincott Williams & Wilkins, 2009) 9th ed.